Published in final edited form as:
J Vasc Interv Radiol. 2010 January ; 21(1): 122. doi:10.1016/j.jvir.2009.09.012.

Radiofrequency Ablation of Lung Tumors in Swine Assisted by a Navigation Device with Pre-procedural Volumetric Planning

Filip Banovac[1,2], **Patrick Cheng**[2], **Enrique Campos-Nanez**[3], **Bhaskar Kallakury**[4], **Teo Popa**[2], **Emmanuel Wilson**[2], **Hernan Abeledo**[3], and **Kevin Cleary**[2]

[1] Department of Radiology, Georgetown University Hospital, Washington, DC, USA

[2] Imaging Science and Information Systems (ISIS) Center, Department of Radiology, Georgetown University, Washington, DC, USA

[3] Engineering Management and Systems Engineering, George Washington University, Washington, DC, USA

[4] Department of Pathology, Georgetown University Hospital, Washington, DC, USA

Abstract

Purpose—The purpose of the study was to develop an image guidance system that incorporates volumetric planning of spherical ablations and electromagnetic tracking of radiofrequency electrodes during insertion.

Methods—Simulated tumors were created in 3 live swine by percutaneously injecting agar nodules into the lung. A treatment plan was devised for each tumor using our optimization software to solve the planning problem. The desired output was the minimum number of overlapping ablation spheres necessary to ablate each tumor and the margin. The insertion plan was executed using the electromagnetic tracking system that guided the insertion of the probe into pre-computed locations. After a 72 hour survival, histopathologic sections of the tissue were examined for cell viability and burn pattern analysis.

Results—A planning algorithm to spherically cover the tumors and the margin was computed. Electromagnetic tracking allowed successful insertion of the instrument and impedance roll-off was reached in all ablations. Depending on their size, the tumors and the tumor margins were successfully covered with 2 to 4 ablation spheres. The image registration error was 1.0 ± 0.64mm. The overall error of probe insertion was 9.4 ± 3.0mm (n=8). Histopathologic sections confirmed successful ablations of the tissue.

Conclusions—Computer assisted RF ablation planning and electromagnetically tracked probe insertion were successful in 3 swine, thus validating the feasibility of electromagnetic tracking assisted tumor targeting. Image mis-registration due to respiratory motion and tissue deformation contributed to the overall error of probe insertion.

Corresponding Author: Filip Banovac at banovac@isis.georgetowm.edu.

A poster of preliminary findings was presented at 2009 SIR meeting.

Introduction

Lung cancer is a leading cause of cancer deaths among men and women in the United States in 2008 (1). Surgical resection remains the only accepted modality with curative potential for early non-small cell lung cancer. However, only about a third of patients are candidates for resection because of concomitant pulmonary disease. Starting in the late 1990's, investigators started to employ minimally invasive percutaneous techniques to treat lung cancer and lung metastases. Goldberg et al. first described successful radiofrequency ablation (RF ablation) in a lung animal model (2). Starting with Dupuy, early reports of clinical applications of RF ablation in therapy of lung malignancies and metastases have emerged (3–6). Lately, RF ablation for treatment of lung tumors has gained acceptance in clinical practice (7–15).

The guiding principle for thermal ablation of the lung is the same as in other organ systems: thermal coagulation of the tissue with cell death. Lungs are well suited for RF ablation since the surrounding air has an insulating effect and concentrates the energy deposition in the tumor (16). Tumor recurrence is one of the shortcomings of lung RF ablation, especially in large lesions. As expected, recurrence in large lung tumors is often at the periphery of the lesion (17). In these larger tumors, a geometric overlap of ablation spheres is employed to "sculpt" a treatment volume. Steinke et al. described the technique for overlapping ablations for large lung tumors and pointed out the technical difficulty in achieving an adequate treatment volume (17). However, guidance techniques to deliver the RF ablation electrode into a precise configuration of overlapping volumes are still not well developed. The mental construct of a 3-dimensional map of the RF ablation electrode placement is highly dependent on the skill of the operator.

Starting with Solomon et al. who described the early uses of electromagnetic instrument tracking for interventional procedures (18–20), the use of this technology has become a topic of investigation. Our group has been developing interventional assist systems based on active electromagnetic (EM) tracking of instruments that could aid in precise delivery of an RF ablation electrode into a target (21,22). Using the power of computer assisted methods for volumetric planning, we developed a physician-assist system that allows for pre-procedural planning and real-time assistance of electrode insertion into predetermined locations in the tumor. This allows volumetric "sculpting" of the ablation zones to cover the tumor and the desired ablative margin. The purpose of this study is to describe our integrated system and the algorithms developed to maximize the volume of tumor destruction with a minimal number of ablation spheres. Furthermore, as a feasibility study, we present the initial results of this approach using a swine lung tumor model.

Materials and Methods

Design of an Electromagnetic Navigation and Treatment Planning System

A computer assisted instrument navigation system was developed which integrated the electromagnetic tracking technology with the guidance and planning software. The working system allowed the operator to load the pre-procedural images, perform off-line tumor segmentation, create a treatment plan, and finally graphically assist the interventional radiologist in inserting the RF ablation electrode into predetermined locations within a swine lung tumor in real-time as shown in Figure 1. The integrated system consists of the components described below.

Electromagnetic Navigation System and the trackable RF ablation stylette—A navigation and guidance system was developed based on a commercially available electromagnetic tracking system (AURORA, Northern Digital Inc., Ontario, Canada) as shown in Figure 2. A modification of the system which we described previously (23,24) allowed the

integration of a EM sensor into a custom-made 15 cm stylet (Traxtal Inc., Ontario, Canada) as seen in Figure 2. The tracked stylet is compatible with a standard 15 cm stylet from the LaVeen Coaxial RF ablation system (Boston Scientific, Natick, MA). This in turn allowed the introducing trocar and the stylet to be tracked on pre-acquired CT images and displayed in real-time as it was inserted toward the target. Once in place, the EM tracked stylet is removed and the RF ablation multi-tined expandable electrode is inserted to perform the burn.

Image guidance software and tumor segmentation—The software used for image guidance was based on the open source software package the Image-Guided Surgical Toolkit (IGSTK) (25). The development of IGSTK was led by our research team and the software provides the basic components needed for rapid prototyping and development of image-guided surgery applications. The graphical user interface shown in Figure 1 displayed the axial and sagittal projections as well as the "birds-eye" view used to visualize the insertion down the length of the RF ablation trocar in real-time as it was being inserted.

The tumor was segmented in a semi-automatic manner using the open source program ITK-SNAP (http://www.itksnap.org/). This same user interface was also employed to allow the interventional radiologist to contour the tumor. Additionally, the user could define the preferred skin entry points. Finally, the user defined the "no-pass" and "no-burn" areas to avoid any puncture or thermal damage to potential interposed organs. All of this information was given to the optimization algorithm described in the next section to create a treatment plan.

Overlapping Sphere Algorithms

Our approach to covering the entire tumor with a series of ablation spheres was based on several guiding objectives. A schematic of the approach is illustrated in Figure 3.

1. Covering the entire tumor plus a predefined ablative margin with a composite of spherical treatment burns
2. Minimizing the number of ablations
3. Minimizing the number of electrode insertion trajectories
4. Avoiding any critical organ transgression or ablation

Mathematical formulations to optimize these concepts were programmed into the system. Finding an adequate compromise between these objectives required the use of goal programming concepts. We utilized an approach where objectives are prioritized and optimized in a sequence and low priority objectives are improved only when such improvements have no effect on higher priority goals. As a practical example, treating the entire tumor would take precedence over minimizing the number of electrode insertion trajectories. Alternatively, avoiding critical organ transgression such as the pericardium, would take precedence over minimizing the number of ablations, etc. The planning software was designed to iterate through these goals until a complete treatment plan was finalized.

Swine Studies

As a proof of concept, a single artificial tumor was created in three separate 35–40 kg Yorkshire swine. The specific sequence of tasks is presented in the flowchart in Figure 4. A typical setup of the EM tracking equipment, the graphical user interface, and the anesthetized animal is shown in Figure 5.

The Animal Care and Use Committee approval was obtained for the study. The anesthetized animal was positioned on the angiography table equipped with cone-beam CT capability. Under general veterinary anesthesia and using a modification of a protocol described by Tsuchida et al. (26), approximately 4 grams of purified agar dissolved in distilled water diluted

10:1 with Omnipaque 300 (Amersham, Piscataway, NJ) was percutaneously injected into the lung parenchyma using a 21-gauge needle. This agar nodule served as a simulated tumor around which desired ablations were planned to achieve a larger compound burn. Subsequently, the animal was pharmacologically paralyzed using pancuronium 0.1 to 0.2 mg/kg. Five surface fiducial markers (MN 3002 multimodality markers; IZI, Baltimore, MD) were placed on the thorax and upper abdomen to serve as registration markers later in the study. They were placed on the skin in the relative proximity of the underlying agar target in order to be in the field of view during the cone-beam CT acquisition. A 20-gauge stylet containing an electromagnetic sensor (MagTrax needle; Traxtal, Ontario, Canada) was inserted into the subcutaneous tissues to serve as an active fiducial that moved with respiration and updated the relative position of the target as shown in Figure 6. The needle shaft of the 20-gauge stylet containing the active fiducial was also secured to the skin with adhesive tape to minimize any retraction of the fiducial during respiration.

Imaging with cone-beam CT—A cone-beam CT of the swine thorax was obtained on the Siemens AXIOM Artis dFA fluoroscopy system (Dyna-CT; Siemens, Erlangen, Germany). During the image acquisition, respiration of the pharmacologically paralyzed animal was suspended for approximately 30 seconds in full ventilatory expiration. Images were then transferred via the DICOM protocol and a network cable to the image guidance workstation.

Image registration—The AURORA electromagnetic tracking system was positioned and enabled, and image registration of the CT space and electromagnetic space was performed using rigid body, paired-point registration (27). Briefly, four surface fiducials were selected in the CT images and then each corresponding fiducial was touched with an actively tracked EM tracked stylet. The position of the subcutaneous needle fiducial (active fiducial) was acquired automatically. The corresponding points in CT space were selected by the physician using the mouse. The image registration based on least-squares method (28) was performed during full expiration of the animal to match the organ position during cone-beam CT acquisition.

Treatment planning and RF ablation instrument navigation—The operating radiologist identified the lung tumor in the images and contoured the margins of the tumor in consecutive axial slices. The algorithm added a 0.5 cm ablative margin around the tumor. A set of acceptable electrode entry points was also selected on the images. Finally, using sequential CT slices, the radiologist added contours around some constraints such as the “no-pass” structures and “no-burn” structures. The algorithm as described above in O*verlapping Sphere Algorithms* then found the best solution for a given treatment problem, choosing a minimum number of target points to achieve the desired ablation.

General anesthesia was maintained by the veterinarian. After activating the EM system, the interventional radiologist inserted the EM tracked trocar/stylet into sequential locations within the lung tumor using only the EM guidance system and the graphical user interface. In sequence, the EM tracked stylet was removed and a 3 cm diameter, multi-tined expandable electrode (LaVeen, Boston Scientific, Natick, MA) was inserted. Each computed target location was reached and ablated before moving to the next location. Each impedance regulated ablation using an RF3000 generator (Boston Scientific, Natic, MA) was completed starting at 10W and adding 5W every 30 seconds until maximum of 150W, for a total of 15 minutes or impedance regulated roll-off, whichever came first. In case of a pneumothorax, an 8 French pigtail thoracostomy was percutaneously inserted and attached to -20 cm water suction.

Swine survival and histopathologic analysis—Each of the animals was survived for 72 hours and then euthanized with Euthasol 1ml/5kg, IV (Virbac Inc., Fort Worth, TX). After necropsy, the lung was fixed in 10% neutral buffered formalin. Sagittal sections of the lung were performed and similarly oriented, and representative sections were taken from each

quadrant of the burned area in each slice. The sections were then embedded in paraffin and 5 μm sections were stained with hematoxylin and eosin stain. Each section was histologically evaluated for tissue viability.

Error Calculations

The registration between the swine anatomy and the cone-beam CT scan was computed after each registration. The fiducial registration error was calculated using the method described by Fitzpatrick et al. (29). The overall error of RF ablation electrode insertion between the pre-planed insertion location and the actual insertion location was calculated in the images using the root mean square method obtained by measuring the tri-axial distances from the final RF ablation electrode position to the projected center of the tumor and calculating the distance as previously described (22).

Results

Two swine survived for 72 hours. The third swine died immediately after the experiment due to respiratory failure related to pathologically proven mycoplasma pneumonia infection. This animal also had a pneumothorax which occurred during the ablation and was treated with insertion of an 8 French pigtail thoracostomy. The pneumothorax was treated successfully; therefore it is unclear whether the pneumothorax also contributed to the respiratory compromise. In this case the necropsy and tissue fixation was performed immediately after death.

A treatment plan to spherically cover the tumors and the ablative margin was computed and is presented in Table 1. In two studies there were two ablations required and in one study four ablations were required. The computation time varied from 18 to 472 seconds. The more complex case requiring four ablations had a larger tumor volume and this significantly increased the computation time. The navigation system aided in successful insertion of the 3 cm RF ablation multi-tined expandable electrode and impedance roll-off was reached in all ablations. The calculated fiducial registration error was 1.0 ± 0.64 mm across all three swine studies. The overall error of RF ablation electrode insertion was 9.4 ± 3.0 mm (n=8).

The histopathologic sections were visually examined throughout the targeted areas. The deflation of the lung during the fixation process sufficiently distorted the anatomy and exact correlation to the planned ablation on the images and the explanted lung was not possible. An aggregate burn area was however confirmed in each case that was sufficiently large to cover the respective tumor of the dimensions listed in Table 1. Reasonable spatial correlation between the planned treatment and the explanted lung was obtained as shown in Figure 7. No agar was found in any of the histologic sections.

Discussion

Tumor recurrence is one of the shortcomings of lung RF ablation, especially in large lesions. As expected, recurrence in large lung tumors is often at the periphery of the lesion (17). Lee et al. found that the tumor size is a major discriminator in achieving complete necrosis where necrosis was attained in 100% of tumors smaller than 3 cm but only in 23% of larger tumors in their series (30). In tumors 3–5 cm in size, they achieved complete coagulation necrosis in only 38%, and tumors greater than 5 cm only 8% achieved complete coagulation necrosis (30). Similar findings were seen in another study where only 39% of tumors larger than 3 cm demonstrated a complete coagulation necrosis (10).

The main impetus for our study was to improve the delivery of the RF ablation electrode into a tumor so that the entire tumor and the desired margin would be more reliably ablated. This

would in turn hopefully achieve better coagulation and better clinical outcomes. The tumor and ablative margins of 0.5 to 1.0 cm were suggested to adequately treat the tumor (31). Although the same margin criteria have not been validated in lung RF ablation, most interventional radiologists try to achieve a margin between 0.5 and 1.0 cm during lung RF ablation. Geometric overlap of ablation spheres is employed to "sculpt" a treatment volume.

In clinical practice, achieving a complete coagulation of a large tumor is difficult. We therefore planned to employ the technique of overlapping ablations to achieve a larger treatment volume and test this concept in a swine tumor model. In liver, this technique and models for overlapping ablations have been well described (32,33). Additionally, Krucker et al. described the use of electromagnetic tracking of instruments in a CT environment to perform biopsies or ablations in 20 patients, thus confirming the clinical feasibility of using this technology (34). However, guidance techniques to deliver the RF ablation electrode into a precise configuration of overlapping volumes are still not well developed. The electromagnetic navigation system allowed us to insert the probe into pre-planned locations within the desired tumor to perform the ablations; however, our RF electrode insertion errors were 9.4 ± 3.0 mm, larger than we hoped. As a comparison, Krucker et al. reported a mean targeting error of 10.4 ± 2.0 mm using electromagnetic instrument guidance in the lung. Their series evaluated positioning accuracy for thermal ablation and biopsy guidance across multiple organ systems (34). Organ and tumor motion resulting from normal physiologic respiration, contributed to significant error during RF electrode insertion. Although our phantom testing done previously had much smaller errors (22), insertion of the RF electrodes into the lung of a live animal proved to be more challenging. Improvements to the optimization software in our future work may also include an iterative solution to probe placements, allowing for re-calculation of subsequent probe positions "on the fly" and taking into account the actual probe position as each burn is completed.

One of the limitations of our study was that image mis-registration contributed to the overall error. The image registration technique that we used relies on rigid body assumptions and does not account for deformation of the organs during breathing, an assumption that is obviously not correct in clinical practice. At this time, deformable (non-rigid) registration is still primarily a research topic. Hawkes et al. have made some progress in this area (35,36). The principal aim of their work has been to devise methods based on non-rigid registration technology to quantify organ motion and use this information to construct a compact computer model of organ motion that is able to predict the three dimensional location of an anatomical target at a point in time with an accuracy that is clinically useful. Recent research has focused on developing techniques for modeling lung and liver motion over the breathing cycle from images acquired using cross sectional imaging for potential application to image-guided lung radiotherapy and RF ablation of liver tumors (37,38). While these approaches are promising, they are still in their early stages, and there is a need for further development of deformable registration and modeling to advance these techniques to the point where they can be clinically useful. Additionally, limitations of this technology in general are mostly related to the alterations of the underlying anatomy during the procedure. Even a small pneumothorax or hemorrhage can alter the anatomic positions of the targets and severely compromise the treatment plan.

Another limitation of our work was the lack of correlation between the lung and tumor anatomy in the images and the lung explants. The lung deflated after explantation and although we tried to fill the airspaces with the formalin solution, the overall volume of the explanted lung was smaller that the physiologic lung seen in the images. This precluded us from making a correlation between the planned position of the respective spherical ablations in the images and those in the explants. Additionally, agar targets diffused inside the lung parenchyma over time, further complicating the correlation between the planned ablations and the histopathologic evaluation. In fact, no agar was found in any of the histopathologic sections,

presumably due to diffusion and vascular and lymphatic washout of agar during the 72 hour survival. That notwithstanding, this study successfully demonstrated the concept of using a computer assisted planning and navigation system to deliver an RF ablation electrode into an artificially created lung tumor of a live animal. Pre-procedural planning and calculation of the minimum number of spheres to cover a tumor of a given volume was successful. The calculations certainly added some time to the overall procedure time, but were not so time consuming to be preclusive. We estimate that the additional time required for pre-procedure set-up and planning was approximately 20 minutes. With further refinement of the image registration methods and ever increasing computer processing speeds, the overall approach may have value in the future of RF ablation.

Acknowledgments

The authors want to thank Neil Glossop, PhD, Traxtal Inc. for designing and manufacturing the electromagnetically trackable stylet.

This research has been funded by the Ernest J. Ring Academic Development Grant sponsored by the Society of Interventional Radiology and in part by U.S. Army grant W81XWH-04-1-007.

The software toolkit ITK-SNAP used in this study was funded by NIH grant R01- EB007195.

References

1. American Cancer Society. Cancer Facts and Figures 2008. Atlanta:
2. Goldberg SN, Gazelle GS, Compton CC, McLoud TC. Radiofrequency tissue ablation in the rabbit lung: efficacy and complications. Acad Radiol 1995;2:776–784. [PubMed: 9419639]
3. Dupuy DE, Zagoria RJ, Akerley W, Mayo-Smith WW, Kavanagh PV, Safran H. Percutaneous radiofrequency ablation of malignancies in the lung. AJR Am J Roentgenol 2000;174:57–59. [PubMed: 10628454]
4. Zagoria RJ, Chen MY, Kavanagh PV, Torti FM. Radio frequency ablation of lung metastases from renal cell carcinoma. J Urol 2001;166:1827–1828. [PubMed: 11586236]
5. Dupuy DE, Mayo-Smith WW, Abbott GF, DiPetrillo T. Clinical applications of radio-frequency tumor ablation in the thorax. Radiographics 2002;22:S259–69. [PubMed: 12376615]
6. Nishida T, Inoue K, Kawata Y, et al. Percutaneous radiofrequency ablation of lung neoplasms: a minimally invasive strategy for inoperable patients. J Am Coll Surg 2002;195:426–430. [PubMed: 12229953]
7. Yasui K, Kanazawa S, Sano Y, et al. Thoracic tumors treated with CT-guided radiofrequency ablation: initial experience. Radiology 2004;231:850–857. [PubMed: 15105453]
8. Belfiore G, Moggio G, Tedeschi E, et al. CT-guided radiofrequency ablation: a potential complementary therapy for patients with unresectable primary lung cancer--a preliminary report of 33 patients. AJR Am J Roentgenol 2004;183:1003–1011. [PubMed: 15385294]
9. Suh RD, Wallace AB, Sheehan RE, Heinze SB, Goldin JG. Unresectable pulmonary malignancies: CT-guided percutaneous radiofrequency ablation--preliminary results. Radiology 2003;229:821–829. [PubMed: 14657317]
10. Akeboshi M, Yamakado K, Nakatsuka A, et al. Percutaneous radiofrequency ablation of lung neoplasms: initial therapeutic response. J Vasc Interv Radiol 2004;15:463–470. [PubMed: 15126656]
11. Gadaleta C, Mattioli V, Colucci G, et al. Radiofrequency ablation of 40 lung neoplasms: preliminary results. AJR Am J Roentgenol 2004;183:361–368. [PubMed: 15269026]
12. Jin GY, Lee JM, Lee YC, Han YM, Lim YS. Primary and secondary lung malignancies treated with percutaneous radiofrequency ablation: evaluation with follow-up helical CT. AJR Am J Roentgenol 2004;183:1013–1020. [PubMed: 15385295]
13. Steinke K, Glenn D, King J, et al. Percutaneous imaging-guided radiofrequency ablation in patients with colorectal pulmonary metastases: 1-year follow-up. Ann Surg Oncol 2004;11:207–212. [PubMed: 14761926]

14. Vansonnenberg E, Shankar S, Morrison PR, et al. Radiofrequency ablation of thoracic lesions: part 2, initial clinical experience--technical and multidisciplinary considerations in 30 patients. AJR Am J Roentgenol 2005;184:381–390. [PubMed: 15671350]
15. Bojarski JD, Dupuy DE, Mayo-Smith WW. CT imaging findings of pulmonary neoplasms after treatment with radiofrequency ablation: results in 32 tumors. AJR Am J Roentgenol 2005;185:466–471. [PubMed: 16037522]
16. Lencioni R, Crocetti L, Cioni R, et al. Radiofrequency ablation of lung malignancies: where do we stand? Cardiovasc Intervent Radiol 2004;27:581–590. [PubMed: 15578133]
17. Steinke K, Glenn D, King J, Morris DL. Percutaneous pulmonary radiofrequency ablation: difficulty achieving complete ablations in big lung lesions. Br J Radiol 2003;76:742–745. [PubMed: 14512336]
18. Solomon SB, White P Jr, Acker DE, Strandberg J, Venbrux AC. Real-time bronchoscope tip localization enables three-dimensional CT image guidance for transbronchial needle aspiration in swine. Chest 1998;114:1405–1410. [PubMed: 9824022]
19. Solomon SB, Magee C, Acker DE, Venbrux AC. TIPS placement in swine, guided by electromagnetic real-time needle tip localization displayed on previously acquired 3-D CT. Cardiovasc Intervent Radiol 1999;22:411–414. [PubMed: 10501894]
20. Solomon SB, Magee CA, Acker DE, Venbrux AC. Experimental nonfluoroscopic placement of inferior vena cava filters: use of an electromagnetic navigation system with previous CT data. J Vasc Interv Radiol 1999;10:92–95. [PubMed: 10872496]
21. Banovac, F.; Glossop, N.; Lindisch, D.; Tanaka, D.; Levy, E.; Cleary, K. Liver Tumor Biopsy in a Respiring Phantom with the Assistance of a Novel Electromagnetic Navigation Device. Medical Image Computing and Computer Assisted Intervention (MICCAI); Tokyo, Japan. 2002. p. 200-207.
22. Banovac F, Tang J, Xu S, et al. Precision targeting of liver lesions using a novel electromagnetic navigation device in physiologic phantom and swine. Med Phys 2005;32:2698–2705. [PubMed: 16193801]
23. Banovac, F.; Jay, M.; Lindisch, D.; Glossop, N.; Cleary, K. Feasibility of Image-Guided Abdominal Interventions Using a Novel Magnetic Position Sensing Device in an Interventional Radiology Suite. In: Lemke, HU., editor. Computer Assisted Radiology and Surgery (CARS). Paris, France: Springer; 2002. p. 1091
24. Glossop, N.; Cleary, K.; Banovac, F. Needle Tracking Using the AURORA Magnetic Position Sensor. Computer Assisted Orthopaedic Surgery (CAOS); 2002 June 19–23; Santa Fe, NM. 2002.
25. Enquobahrie A, Cheng P, Gary K, et al. The image-guided surgery toolkit IGSTK: an open source C ++ software toolkit. J Digit Imaging 2007;20 (Suppl 1):21–33. [PubMed: 17703338]
26. Tsuchida M, Yamato Y, Aoki T, Watanabe T, Koizumi N, Emura I, et al. CT-guided agar marking for localization of nonpalpable peripheral pulmonary lesions. Chest 1999;116:139–143. [PubMed: 10424517]
27. Peters, T.; Cleary, K. Image-guided interventions: technology and applications. Springer; 2008.
28. Arun KS, Huang TS, Blostein SD. Least squares fitting of two 3D sets. IEEE Trans. Pattern Analysis and Mach. Intell 1987;9:698–700.
29. Fitzpatrick JM, West JB, Maurer CR Jr. Predicting error in rigid-body point-based registration. IEEE Trans Med Imaging 1998;17:694–702. [PubMed: 9874293]
30. Lee JM, Jin GY, Goldberg SN, et al. Percutaneous radiofrequency ablation for inoperable non-small cell lung cancer and metastases: preliminary report. Radiology 2004;230:125–134. [PubMed: 14645875]
31. Gazelle GS, Goldberg SN, Solbiati L, Livraghi T. Tumor ablation with radio-frequency energy. Radiology 2000;217:633–646. [PubMed: 11110923]
32. Chen MH, Yang W, Yan K, et al. Large liver tumors: protocol for radiofrequency ablation and its clinical application in 110 patients--mathematic model, overlapping mode, and electrode placement process. Radiology 2004;232:260–271. [PubMed: 15166323]
33. Dodd GD, Frank MS, Aribandi M, Chopra S, Chintapalli KN. Radiofrequency thermal ablation: computer analysis of the size of the thermal injury created by overlapping ablations. AJR Am J Roentgenol 2001;177:777–782. [PubMed: 11566672]

34. Krücker J, Xu S, Glossop N, et al. Electromagnetic Tracking for Thermal Ablation and Biopsy Guidance: Clinical Evaluation of Spatial Accuracy. Journal of Vascular and Interventional Radiology 2007;18:1141–1150. [PubMed: 17804777]

35. Hawkes D, Barratt D, Blackall J, Chandler A, McClelland J, Penney G. Computational models in image guided interventions. Conf Proc IEEE Eng Med Biol Soc 2005;7:7246–7249. [PubMed: 17281952]

36. Hawkes DJ, Barratt D, Blackall JM, et al. Tissue deformation and shape models in image-guided interventions: a discussion paper. Med Image Anal 2005;9:163–175. [PubMed: 15721231]

37. Blackall JM, Ahmad S, Miquel ME, McClelland JR, Landau DB, Hawkes DJ. MRI-based measurements of respiratory motion variability and assessment of imaging strategies for radiotherapy planning. Phys Med Biol 2006;51:4147–4169. [PubMed: 16912374]

38. McClelland JR, Blackall JM, Tarte S, et al. A continuous 4D motion model from multiple respiratory cycles for use in lung radiotherapy. Med Phys 2006;33:3348–3358. [PubMed: 17022231]

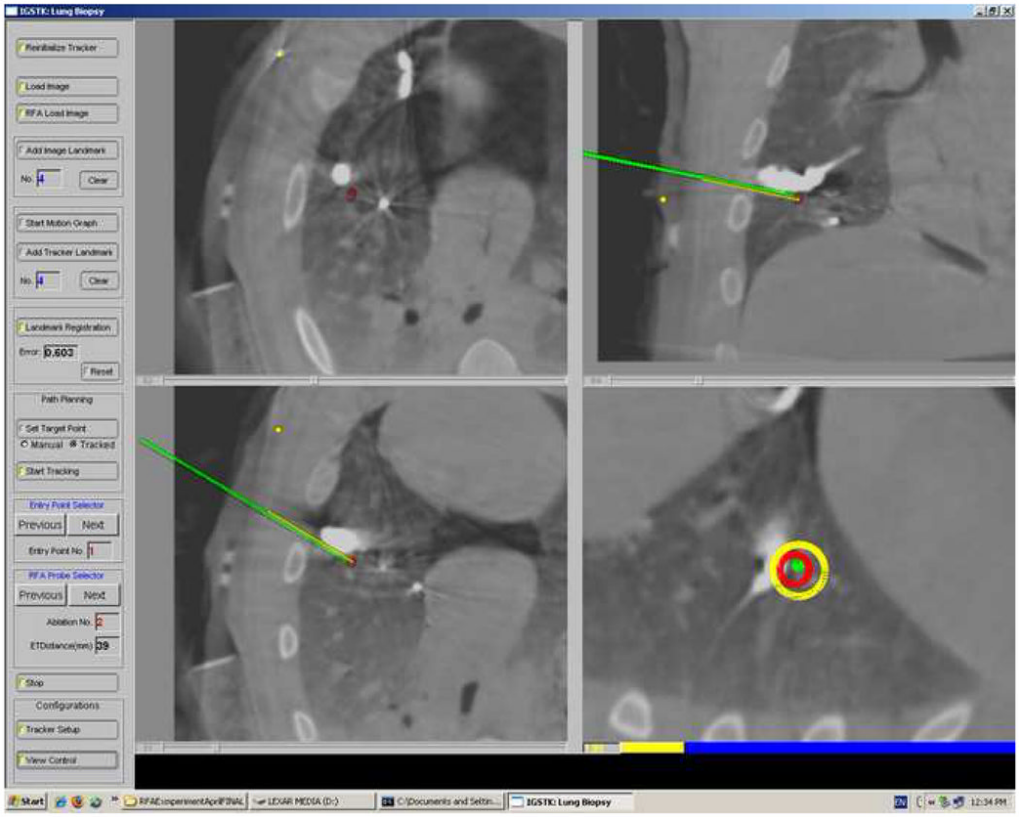

Figure 1.

A four-quadrant view of the graphical user interface showing the tracked instrument as it is advanced towards a target along a planned trajectory. The axial view (top left), sagittal view (top right), off-sagittal view (bottom left) and “birds-eye” targeting view (bottom right) are shown. The “birds-eye” view is used by the operator by aligning the concentric circles during instrument insertion thus confirming that the insertion is along the pre-planned trajectory.

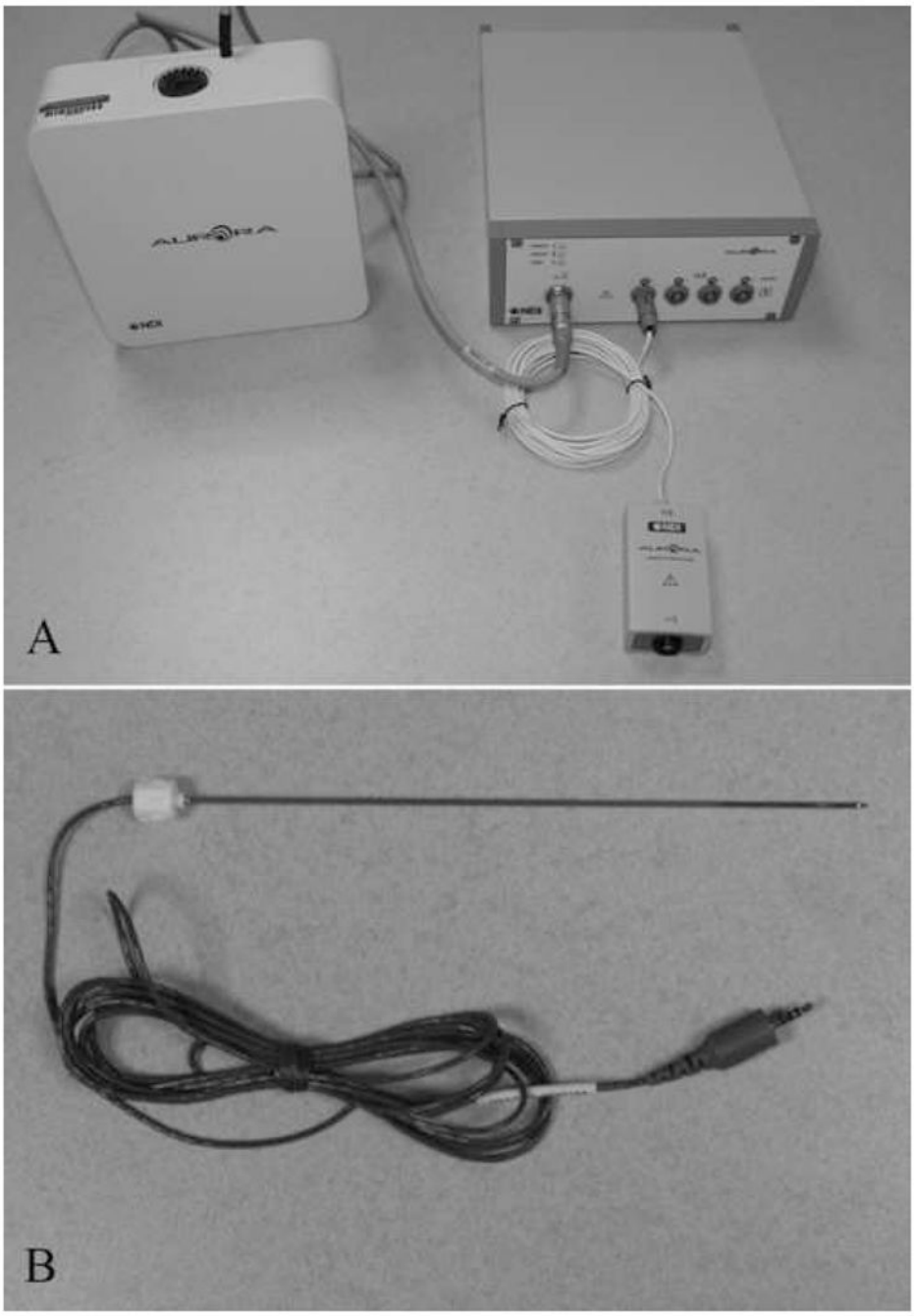

Figure 2.

a) The electromagnetic tracking system consists of a field generator (left), a control unit (right), and a sensor interface device (bottom right). **b)** The magnetic sensor is incorporated into the tip of a tracked stylet. Electrical leads from the stylet are attached to the sensor interface unit.

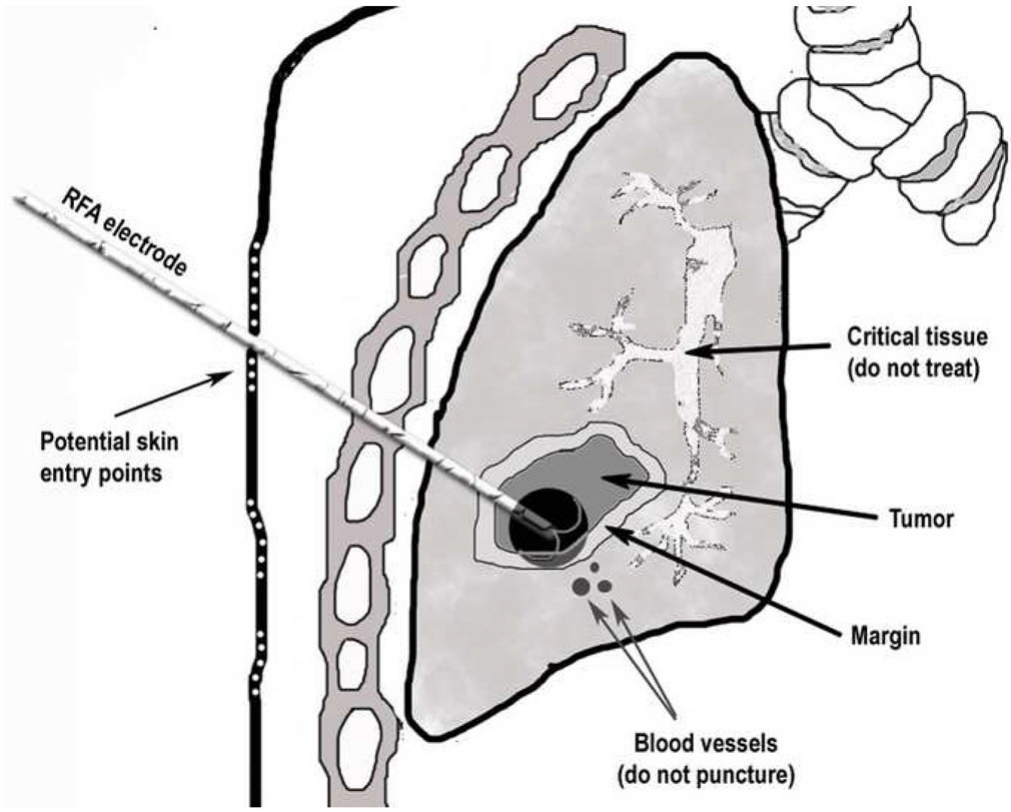

Figure 3.
An illustration of a single treatment where the ablation only covers a portion of the tumor. The RF ablation electrode trajectory would subsequently be recomputed according to the ablation plan to cover the entire tumor and the desired margin. User defined skin entry points are chosen to avoid rib interposition. The algorithm accounts for the location of user-defined critical organs and structures and calculates the best subsequent RF ablation electrode position to optimize the aggregate ablation volume.

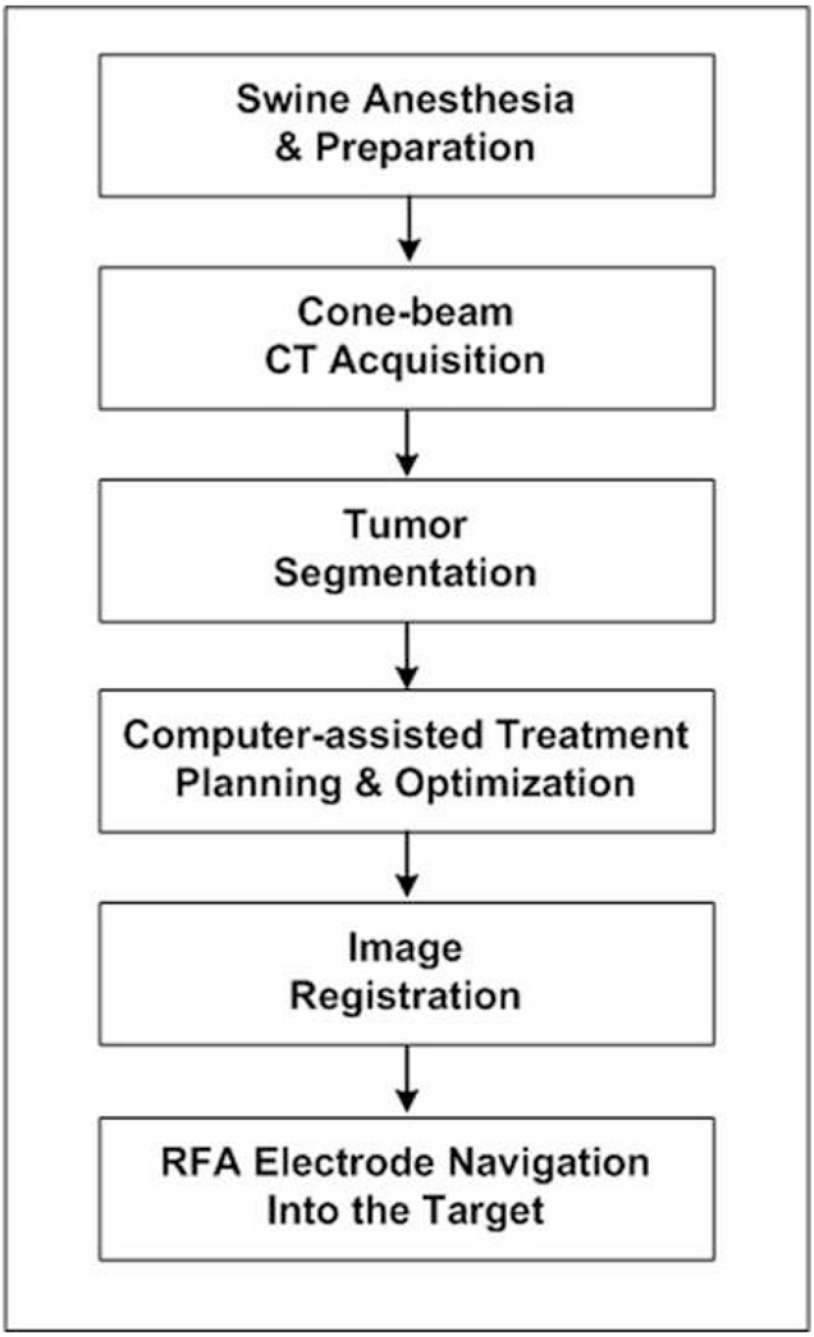

Figure 4.
Typical workflow during an EM guided ablation during swine studies.

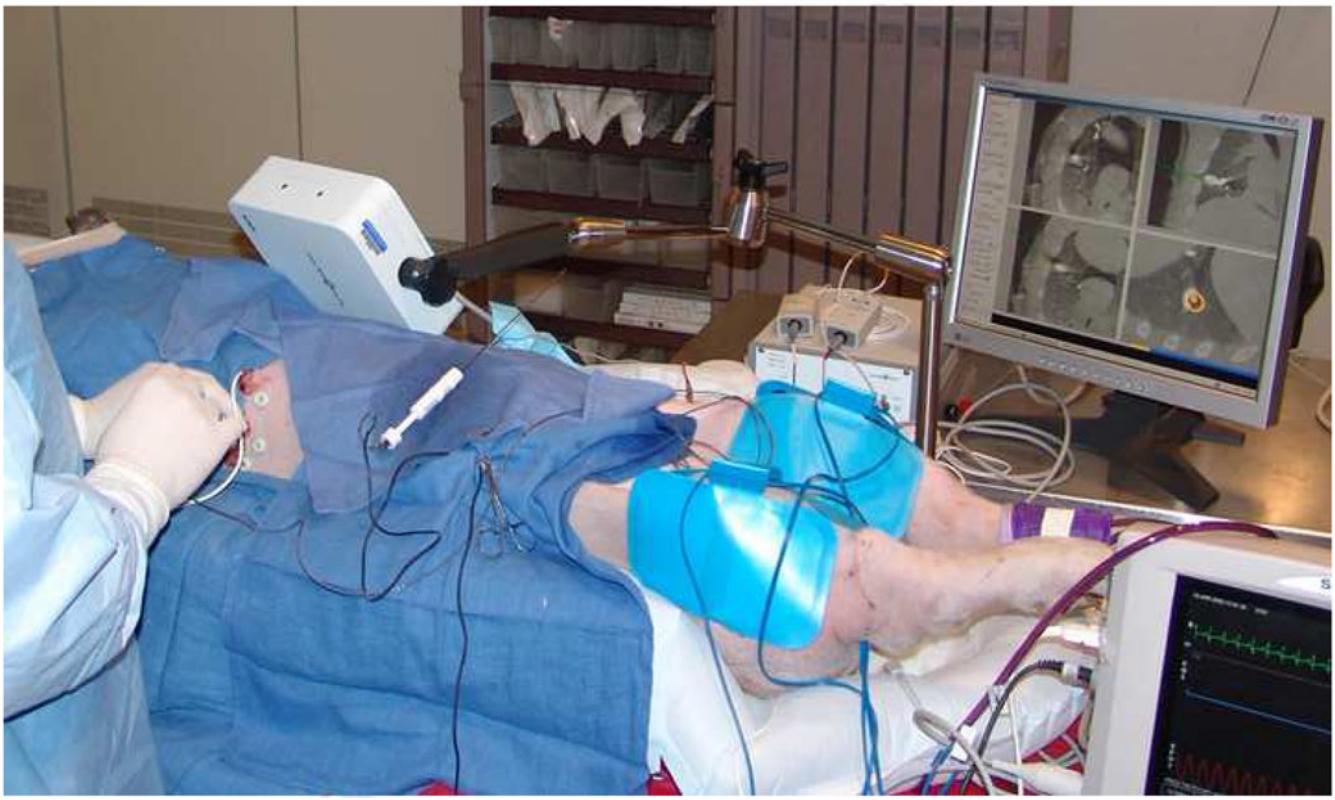

Figure 5.
The electromagnetic field generator is shown above the anesthetized animal as it would be positioned during a typical experimental setup. The user is advancing an EM tracked trocar/stylet into the pre-planned target using only the graphical user interface (top right) without real-time imaging.

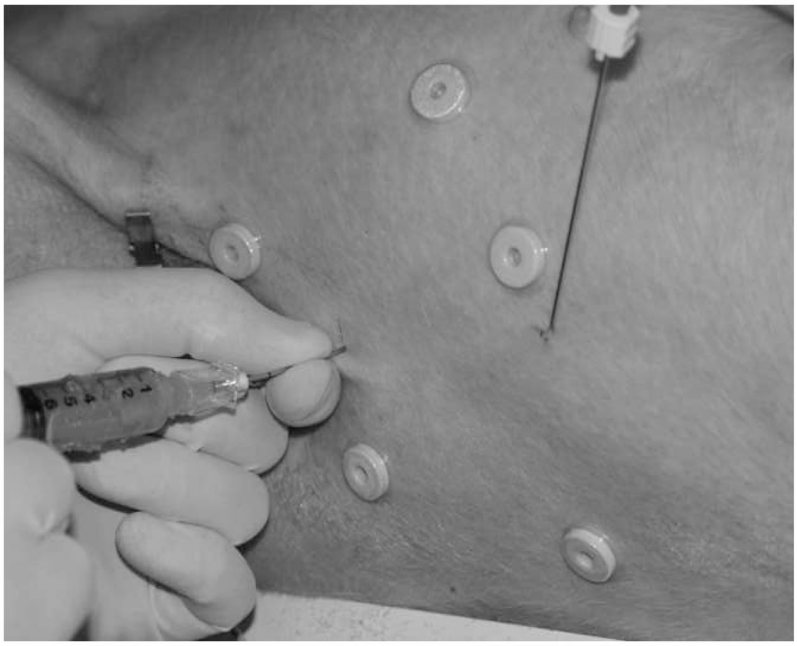

Figure 6.
Percutaneous agar injection used to create a tumor target is shown. Five circular skin fiducials are seen on the skin and serve as registration markers. A 20-gauge stylet (top right) containing an electromagnetic sensor in its tip was inserted into the chest wall of the animal. This sensor is active and its position is read by the EM system in real time. This allows the user to track the respiration induced motion during instrument insertion.

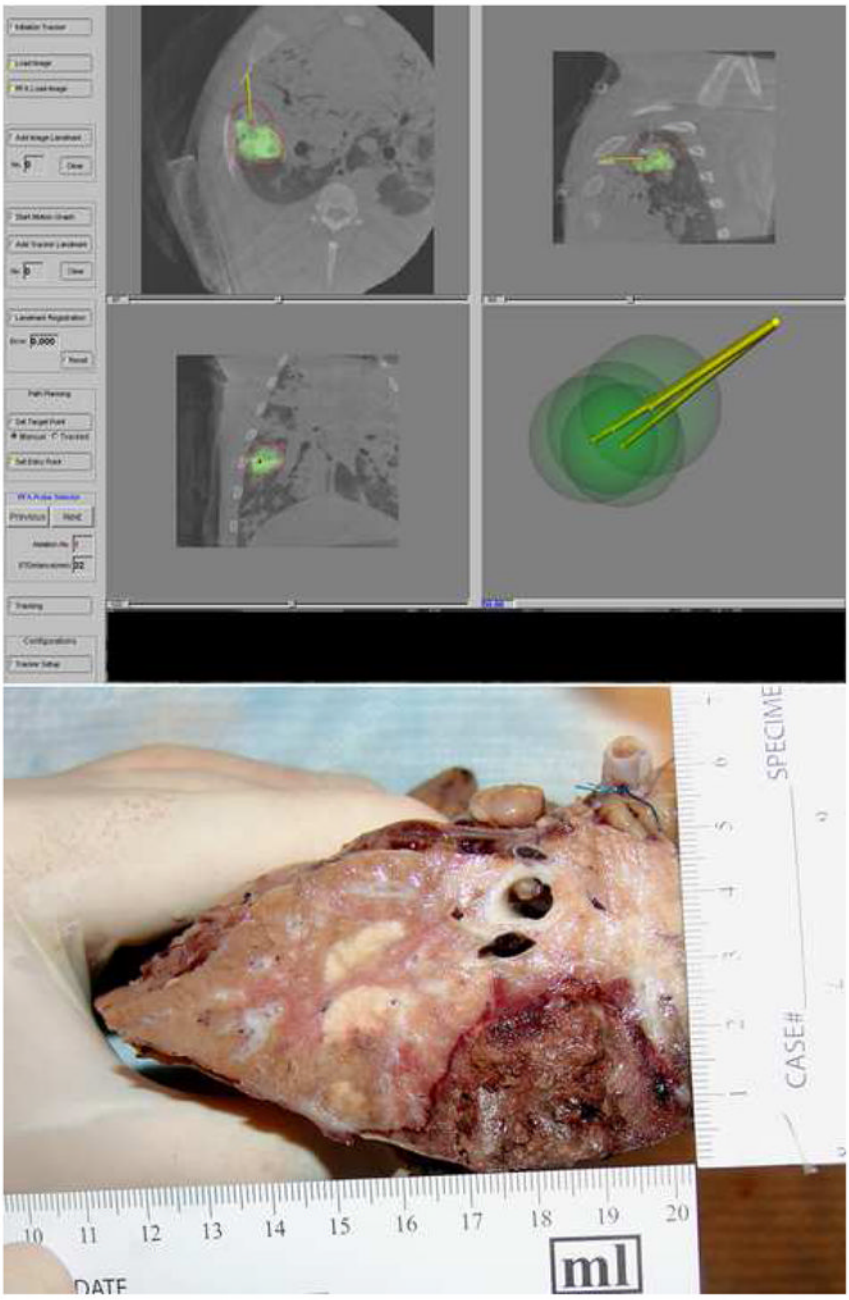

Figure 7.

A four quadrant graphical user interface shows a composite treatment plan that includes four spherical ablations to cover the tumor. The planned treatment margins extend to the pleural surface because of the peripheral position of the tumor (top left). Likewise, a cross section of the explanted lung shows the extension of the coagulation to the pleural surface (bottom) suggesting correct anatomic correlation with the planned treatment.

Table 1

Sizes of tumors and corresponding treatment parameters

Swine	Tumor size (mm)	RF electrode trajectories	Ablation Spheres	Computation Time (s)
1	38 × 30 × 38	2	4	472
2	27 × 15 × 10	2	2	197
3	31 × 17 × 15	2	2	18